Dimer impurity scattering, reconstructed Fermi-surface nesting, and density-wave diagnostics in iron pnictides

Jian Kang and Zlatko Tešanović

Phys. Rev. B **85**, 220507 — Published 26 June 2012

DOI: 10.1103/PhysRevB.85.220507

Dimer Impurity Scattering, Reconstructed Nesting and Density-Wave Diagnostics in Iron Pnictides

Jian Kang[1] and Zlatko Tešanović[1]

[1] *Institute for Quantum Matter and Department of Physics & Astronomy, The Johns Hopkins University, Baltimore, MD 21218*

(Dated: June 14, 2012)

While the impurity-induced nanoscale electronic disorder has been extensively reported in the underdoped iron pnictides, its microscopic origins remain elusive. Recent STM measurements reveal a dimer-type resonant structure induced by cobalt doping. These dimers are randomly distributed but uniformly *aligned* with the antiferromagnetic a-axis. Theory of the impurity-induced quasiparticle interference patterns is presented that shows the local density of states developing an oscillatory pattern characterized by both geometry and orbital content of the *reconstructed* Fermi pockets, occasioned by the pocket density wave (PoDW) order along the b-axis. This pattern breaks the C_4 symmetry and its size and orientation compare well with the dimer resonances found in the STM experiments, hinting at the presence of "hidden" PoDW order. More broadly, our theory spotlights such nanoscale structures as a useful diagnostic tool for various forms of order in iron pnictides.

The iron pnictide high-T_c superconductors[1,2] exhibit several remarkable features[3]. Among them are the proximity and interplay of antiferromagnetism (AFM) and a structural transition[4,5], manifested by anisotropy in electronic properties[6–11]. Various experiments reveal strong correlation between these two transitions[12,13]. A prevalent explanation is that the structural transition results from the fluctuations of incipient AFM order[14,15]. Alternatives include the key role of orbital degrees of freedom[16] and, in particular, the proposal that the structural transition originates from the pocket density-wave (PoDW)[17] in parent compounds, a "hidden" order responsible for orbital ferromagnetism.

Recent STM experiments observe the nematic-type electronic formations developing around dopant atoms[9,18]. These formations appear as "dimer resonances," with two neighboring peaks separated by $\sim 6-8$ lattice spacings. Importantly, the dimers are oriented *along* the a-axis of the pnictides' unidirectional AFM order. In this paper, we show that both the appearance of dimer resonances and their size and orientation provide a direct insight into the electronic structure and correlations in iron pnictides. In this regard, the properties of such dimers can serve as a diagnostic tool to unravel the nature of the underlying microscopic ground state and the sequence of Fermi surface reconstructions left in the wake of various itinerant density-wave (DW) orderings[19].

These are our main results: the dimer resonance[9,18] is a consequence of the new type of "reconstructed" nesting[20] characterized by the wavevector $\vec{q}_a \approx (0.4\pi, 0)$. Such nesting tendency is manifest in our detailed calculations within the three orbital model[21], where $\vec{q}_a$ – associated with the short axis of the elliptical electron pocket – emerges as a prominent feature of the reconstructed band structure, itself occasioned by the transition from the paramagnetic phase to the PoDW. Specifically: *i)* In the paramagnetic phase, the Fermi pocket is far from any nesting at $\vec{q}_a$. Consequently, no resonances appear; *ii)* As PoDW is formed, the electron pocket is itself deformed while, simultaneously, sections of the reconstructed hole pockets become flatter as the PoDW order parameter increases. This gives rise to the "reconstructed" nesting at $\vec{q}_a$; *iii)* $\vec{q}_a$ is *perpendicular* to PoDW, producing the real-space dimer pattern breaking the C_4 symmetry. The resonant pattern arises when randomly distributed dopant impurities induce two peaks in the local density of states (LDOS), *both their separation and direction set by* $\vec{q}_a$; *iv)* When PoDW and SDW coexist, two nesting vectors $q_a \approx (0.4\pi, 0)$ and $q_b \approx (0, 0.4\pi)$ emerge from the reconstructed pockets. With e_y and e_x coupled to the inner and outer hole pockets, h_2 and h_1, respectively, the susceptibility near $\vec{q}_a$ remains much larger than its counterpart near $\vec{q}_b$. Again, the C_4 symmetry is broken resulting in dimer patterns observed in[9,18].

We now supply the details behind the above physical picture. Experiments and theoretical calculations indicate that iron pnictides contain four disconnected Fermi surface pockets (Fig. 1[22])[23]. Additional parts of the Fermi surface are present in some materials[23] but this is not important for the physics discussed here. When two hole pockets closely match two electron pockets, as is the case in many iron pnictide parent compounds[23], the geometric nesting favors formation of two DWs[17]: PoDW partially gaps e_y and one hole pocket and induces structural transition, while e_x and the remaining hole pocket form the partially gapped SDW. The theory[17] naturally explains the proximity of the two transitions and accounts for the observed orbital ferromagnetism.

While geometric nesting tendencies are important[22], they are not the complete story: the orbital content of the Fermi pockets must be considered as well[26]. Here, we start with a simplified geometric model allowing for an analytic glance at the physics and then fortify the results within a detailed numerical follow-up employing three-orbital content[21], known to capture the main features of real materials[23]. We model the Fermi pockets as:

$$\epsilon_{h_1,h_2}(\vec{k}) = \epsilon_0 - \frac{k^2}{2m}$$

$$\epsilon_{e_x}(\vec{k}) = \frac{(k_x-\pi)^2}{2m_a} + \frac{k_y^2}{2m_b} - \epsilon_0 \ ; \ \epsilon_{e_y} = \epsilon_{e_x}(k_x \leftrightarrow k_y) \quad (1)$$

with $m_a > m > m_b$, so that the two DWs are partially gapped when order parameters Δ_{PoDW} and Δ_{SDW} are small. e_y and e_x bands are related by 90° rotation. To simplify the analytic calculation, we assume that h_1 and h_2 are isotropic and have the same dispersion relations.

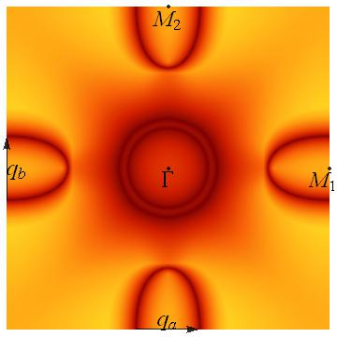

FIG. 1. (Color online) Fermi pockets in the UBZ of iron-pnictides. Two hole pockets h_1 and h_2 are centered at the $\Gamma = (0,0)$ point. The elliptical electron pockets e_x and e_y are centered at $\vec{M}_1 = (\pi, 0)$ and $\vec{M}_2 = (0, \pi)$, respectively. h_1, h_2, e_x, and e_y pockets exhibit strong nesting tendencies in many parent compounds. Here, we propose that the resonant electronic structure arises due to the "reconstructed" nesting with the wave vector $\sim \vec{q}_a$, the shorter axis of the e_y pocket.

It is known that static charge/spin susceptibilities contain peaks around the nesting vectors $\vec{M}_1 = (\pi, 0)$ and $\vec{M}_2 = (0, \pi)$ in the above noninteracting model, implying tendency to DW formation in moderately correlated iron pnictides[22]. Initially, by ignoring the orbital content at the Fermi level within[24], we can determine the analytic form for such geometric susceptibility at $T = 0$, within a *single* elliptical electron pocket (1):

$$\chi(q_x, q_y) = 2\int \frac{\mathrm{d}^2k}{(2\pi)^2} \frac{n_f(\epsilon(\vec{k})) - n_f(\epsilon(\vec{k}-\vec{q}))}{\epsilon(\vec{k}-\vec{q}) - \epsilon(\vec{k}) + i0^+}$$

$$= \begin{cases} \frac{\sqrt{m_a m_b}}{4\pi} & \text{if } \frac{q_x^2}{2m_a} + \frac{q_y^2}{2m_b} < 4\epsilon_0. \\ \frac{\sqrt{m_a m_b}}{4\pi}\left[1 - \sqrt{1 - \frac{4\epsilon_0}{\frac{q_x^2}{2m_a} + \frac{q_y^2}{2m_b}}}\right] & \text{if } \frac{q_x^2}{2m_a} + \frac{q_y^2}{2m_b} > 4\epsilon_0. \end{cases}$$

$\chi(\vec{q})$ is effectively a constant for $\vec{q}/2$ within the pocket, and decreases slowly as $\vec{q}/2$ moves outside. Consequently, $\chi(\vec{q})$ contains only an unremarkable ridge instead of a peak, implying no resonance around $\vec{q}_a$ in the normal state of such a simple geometric model. These features of geometric nesting are echoed in a realistic calculation with full orbital content[22,24]:

$$\chi(\vec{r}, \vec{r}') = \langle \rho(\vec{r})\rho(\vec{r}')\rangle = \sum_{\alpha,\beta} \langle d_\alpha^\dagger(\vec{r}) d_\alpha(\vec{r}) d_\beta^\dagger(\vec{r}') d_\beta(\vec{r}')\rangle$$

$$= -\frac{2}{N^2} \sum_{k_i,\mu_i} \langle d_{\mu_1}^\dagger(\vec{k}_1) d_{\mu_4}(\vec{k}_4)\rangle \langle d_{\mu_3}^\dagger(\vec{k}_3) d_{\mu_2}(\vec{k}_2)\rangle \langle \mu_1, \vec{k}_1 | \mu_2, \vec{k}_2\rangle$$

$$\langle \mu_3, \vec{k}_3 | \mu_4, \vec{k}_4\rangle \exp\left(i(\vec{k}_2 - \vec{k}_1)\vec{r} + i(\vec{k}_4 - \vec{k}_3)\vec{r}'\right) \ , \quad (2)$$

where α, β denote d orbitals and μ_is are the band indices. In the paramagnetic phase, the Green's function $\langle d_{\mu_i}(\vec{k}_i, \omega_n) d_{\mu_j}^\dagger(\vec{k}_j, \omega_n)\rangle$ is finite only if $\vec{k}_i = \vec{k}_j$ and $\mu_i = \mu_j$ and thus Eq. (2) gives

$$\chi(\vec{q}) = \frac{2}{N} \sum_{\vec{k},\mu,\nu} \frac{\left|\langle \mu, \vec{k}+\vec{q} | \nu, \vec{k}\rangle\right|^2 (n_f(\epsilon_\nu) - n_f(\epsilon_\mu))}{\epsilon_\mu(\vec{k}+\vec{q}) - \epsilon_\nu(\vec{k}) + i0^+}. \quad (3)$$

The factor of 2 in (2) is due to spin and $n_f(\epsilon)$ is the Fermi distribution function. Again, we find nesting peaks at $(\pi, 0)$ and $(0, \pi)$ but no enhanced structure near $\vec{q}_a$.

The situation changes once the DW order is established. Within a PoDW, which is the leading DW instability of Ref.[17], the electron pocket e_y couples with one of the hole pockets; in the following, we assume this is h_2. The reconstructed Fermi surface is shown in Fig. 2. $\chi(\vec{q}_a)$ now increases reflecting the nesting between the *reconstructed* electron pockets: e_y deformation promotes $\vec{q}_a$ to a "reconstructed" nesting vector, connecting separate portions of two small e pockets, as depicted in Fig. 2. When Δ_{PoDW} is small, $\vec{q} = \vec{q}_a$ is a local maximum of $\chi(\vec{q})$, with a strong peak when the nesting is optimized, i.e. $\left(\partial^2\lambda/\partial k_y^2\right)_{k_x = \pm q_a/2, k_y = 0} = 0$, λ being the energy of the reconstructed h pocket. Within our simple model (1)

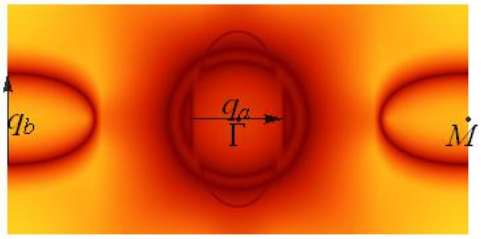

FIG. 2. (Color online)As PoDW order develops, the Fermi surface reconstructs, and e_y and the inner hole pocket h_2 are deformed. The curvature along e_y decreases, leading to the "reconstructed" nesting at q_a, the short axis of e_y pocket. This reconstructed nesting is absent in the paramagnetic phase, but becomes pronounced as Δ_{PoDW} increases.

$$\Delta_{opt} = \epsilon_0 \frac{m - m_b}{m_a + m_b} \sqrt{\frac{m_a}{m}} \quad (4)$$

optimizes nesting. For $\Delta_{PoDW} \ll \Delta_{opt}$, χ increases by

$$\delta\chi(\vec{q}_a) = \chi_{PoDW}(\vec{q}_a) - \chi_{para}(\vec{q}_a)$$

$$\approx \frac{\sqrt{2m_a m_b}}{\pi^2} \left(\frac{m_a - m}{m_a - m_b}\right)^{\frac{1}{4}} \left(\frac{\Delta}{\epsilon_0}\right)^2 \frac{m(m+m_a)}{(m-m_b)^2} \ , \quad (5)$$

while, for $\Delta_{PoDW} = \Delta_{opt}$,

$$\delta\chi(\vec{q}_a) \approx \frac{1}{\pi^2}\left(\frac{\Delta k}{v_F^3\beta}\right)^{1/4} \quad (6)$$

$$\Delta k \approx \sqrt{\frac{\epsilon_0}{m+m_b}}\frac{m_a-m_b}{m_a+m_b}(m-m_b) \quad (7)$$

$$v_F = \sqrt{\frac{2\epsilon_0}{m_b}}\frac{m_a-m_b}{\sqrt{(m+m_a)(m_a+m_b)}} \quad (8)$$

$$\beta = \left(\frac{1}{m}+\frac{1}{m_a}\right)\frac{m_a+m_b}{32\epsilon_0 m_b(m-m_a)} \left[1-\frac{1}{4}\left(\frac{m_a-m}{m+m_b}\right)^2\right] . \quad (9)$$

Δk is width of the reconstructed h pocket, v_F is the Fermi velocity $\parallel \hat{x}$, $\vec{k} = \vec{q}_a/2$, and $\beta = \left(\partial^4\epsilon/\partial k_y^4\right)_{k_x=q_a/2,k_y=0}$.

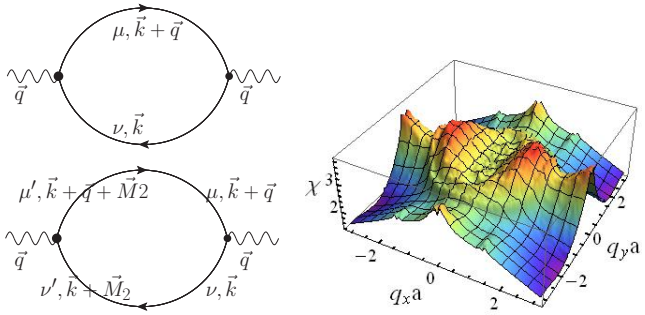

FIG. 3. (Color Online)(*left*) Feynman diagrams for χ^c in the PoDW phase. All other diagrams cancel out. (*right*) $\chi^c(\vec{k})$ with $\Delta_{PoDW} = 20meV$ in the realistic three orbital model. The original peaks at $(0, \pm\pi)$ in paramagnetic phase are suppressed by finite Δ_{PoDW}. Instead, $\chi(\vec{k})$ contains a plateau centered at $\vec{q}_a \approx (\pm 0.4\pi, 0)$, breaking the C_4 symmetry. This plateau arises from the "reconstructed" nesting at q_a.

Again, we fortify the above picture with the realistic calculation of charge susceptibility $\chi^c(\vec{q})$ within the three orbital model. In the PoDW state, $\langle d_{\mu_i}(\vec{k}_i, \omega_n) d^\dagger_{\mu_j}(\vec{k}_j, \omega_n)\rangle$ is finite only if $\mu_i = \mu_j$ and $\vec{k}_i = \vec{k}_j$ or $(\mu_i, \mu_j) = (e_y, h_2)$ and $\vec{k}_i = \vec{k}_j + (0, \pi)$. Fig. 3 displays Feynman diagrams contributing to $\chi^c(\vec{k})$. Additional diagrams, composed of one normal and one anomalous Green's function, break time reversal symmetry and cancel out upon summation over $\vec{k}$. χ^c is calculated within the three orbital model and shown in Fig. 3. Evidently, a high plateau around $(\pm 0.4\pi, 0)$ arises due to the "reconstructed nesting" at vector $\vec{q}_a$. This is qualitatively consistent with the results in Eq. (6) for the simple model (1). In addition, the original peaks at $\vec{M}_2 = (0, \pm\pi)$ are suppressed due to formation of PoDW.

At low T, Ref.[17] predicts coexistence of PoDW and SDW, and therefore, leads to two "reconstructed" nesting vectors, $\vec{q}_a$ and $\vec{q}_b$, related by 90° rotations. If $\Delta_{PoDW} \neq \Delta_{SDW}$, the C_4 symmetry is already broken by this unequal pairing. In[17], $\Delta_{PoDW} > \Delta_{SDW}$ and this naturally leads to $\chi(\vec{q}_a) > \chi(\vec{q}_b)$. When $\Delta_{PoDW} = \Delta_{SDW}$, however, the difference between $\chi(\vec{q}_a)$ and $\chi(\vec{q}_b)$ could still arise from distinct orbital content of Fermi pockets. To illustrate the effect of orbital content, we assume[23]

$$h_1 = \cos(\theta) d_{yz} + \sin(\theta) d_{xz} \quad (10)$$

$$h_2 = \cos(\theta) d_{xz} - \sin(\theta) d_{xz} \quad (11)$$

$$e_x = d_{yz} \quad e_y = d_{xz} , \quad (12)$$

where θ is the polar angle at the Fermi pocket.

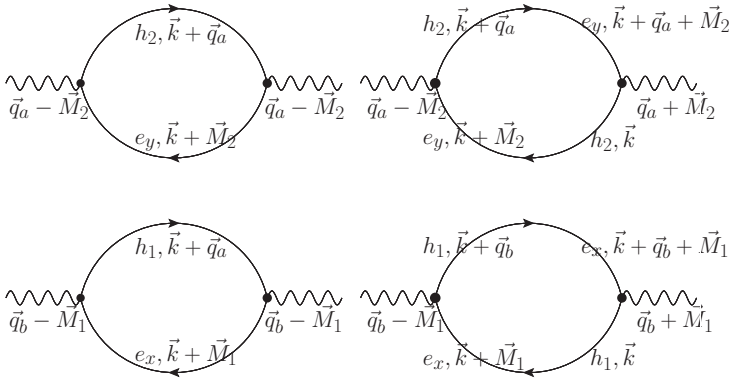

FIG. 4. C_4 symmetry is broken due to orbital content. Only the most significant diagrams contributing to the difference between $\chi(\vec{q}_b)$ and $\chi(\vec{q}_a)$ are displayed. The upper and lower two contribute to $\chi(\vec{q}_a)$ and $\chi(\vec{q}_b)$, respectively. This difference arises from the vertex, which includes orbital overlaps between incoming and outgoing fermions. The diagrams which have C_4 symmetric partners are not shown.

Fig. 4 shows the Feynman diagrams contributing to the susceptibility difference $\delta\chi = \chi(\vec{q}_a + \vec{M}_2) - \chi(\vec{q}_b + \vec{M}_1)$. Quantitatively, $\delta\chi$ is dominated by the first diagram:

$$\delta\chi \approx \int \frac{\mathrm{d}\vec{k}_1}{(2\pi)^2}(\cos^2\theta(\vec{k}+\vec{q}) - \sin^2\theta(\vec{k}+\vec{q})) u^2(\vec{k}+\vec{q})v^2(\vec{k})\frac{n_f(\lambda(\vec{k})) - n_f(\lambda(\vec{k}+\vec{q}))}{\lambda(\vec{k}+\vec{q}) - \lambda(\vec{k})}. \quad (13)$$

The vertex factors $\cos^2\theta(\vec{k}+\vec{q})$ and $\sin^2\theta(\vec{k}+\vec{q})$ come from the orbital component of the charge density $\rho(\vec{r})$ when calculating $\chi(\vec{q}_a)$ and $\chi(\vec{q}_b)$, respectively,

$$u^2(\vec{k}) = \frac{1}{2}\left(1 + \frac{\left(\epsilon_h(\vec{k}) - \epsilon_e(\vec{k}+\vec{M})\right)/2}{\sqrt{\left((\epsilon_h(\vec{k}) - \epsilon_e(\vec{k}+\vec{M}))/2\right)^2 + \Delta^2}}\right),$$

$$v^2(\vec{k}) = 1 - u^2(\vec{k}) ,$$

n_f is the Fermi function, and λ is the energy of the reconstructed, partially gapped fermions. The other diagrams give similar contributions, with different vertices.

It is now difficult to get an analytic expression for $\delta\chi$ even within the model (1). However, for $\Delta_{PoDW} = \Delta_{SDW} = \Delta_{opt}$ in (4) and at $T = 0$:

$$\delta\chi \approx \frac{1}{\pi^2}\left(\frac{\Delta k}{v_F^3\beta}\right)^{\frac{1}{4}}\frac{\sqrt{m_a m_b(m-m_b)(m_a+m)}}{m(m_a+m_b)}, \quad (14)$$

with δk, v_f and β from Eqs. (7–9). The anisotropy is determined by the choice of coupling between the e and h pockets: $\chi(\vec{q}_a + \vec{M}_2) > (<)\chi(\vec{q}_b + \vec{M}_1)$ when e_y and e_x couple to $h_2(h_1)$ and $h_1(h_2)$, respectively[25].

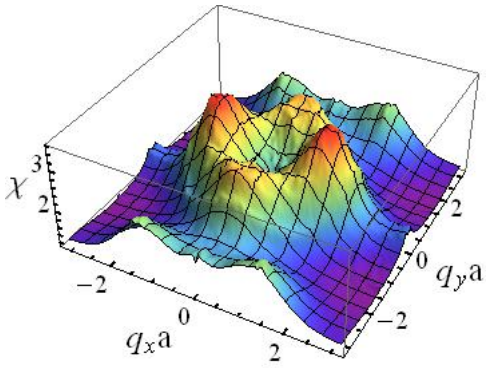

FIG. 5. (Color Online)$\chi^c(\vec{k})$ with $\Delta_{PoDW} = 20meV$ and $\Delta_{SDW} = 15meV$ within the three orbital model. The original peaks around $(0, \pm\pi)$ and $(\pm\pi, 0)$ in paramagnetic phase are suppressed due to finite Δ_{PoDW}. In addition, two small peaks emerge around $(\pm 0.4\pi, \pm\pi)$, breaking the C_4 symmetry.

Again, we follow up with the realistic calculation of $\chi^c(\vec{q})$ based on the three orbital model. The results are displayed in Fig. 5. The peaks at the nesting vectors $\vec{M}_1$ and $\vec{M}_2$ are suppressed due to the PoDW and SDW. Evidently, $\chi(\vec{k})$ breaks the C_4 symmetry, as expected.

STM experiments reveal an anisotropic electronic dimer structure developing when the iron pnictide is doped with cobalt[18]. Our theory of reconstructed nesting can account for this phenomenon, by considering the impurity-induced quasiparticle interference in the parent compounds. First, the local potential of the cobalt atom is $H_{imp} = \sum_{\sigma,\alpha}(V_s^\alpha + \sigma V_m^\alpha) d_\alpha^\dagger(\vec{r}) d_\alpha(\vec{r})$, where V_s and V_m are the nonmagnetic and the magnetic parts of the impurity potential, respectively, and are given for each orbital α in[26]. The LDOS with a single impurity is:

$$\rho(E, \vec{r}') = -\frac{1}{\pi} Im \sum_{\alpha,\sigma} G_{\alpha\alpha,\sigma}(i\omega \longrightarrow E + i0^+, \vec{r}', \vec{r}')$$

$$G_\sigma(i\omega, \vec{r}', \vec{r}') = G_0(\vec{r}', \vec{r}') + G_0(\vec{r}', \vec{r}) V_{imp} G_0(\vec{r}, \vec{r}') \quad (15)$$

$$V_{imp} = H_{imp}(1 - G_0 H_{imp})^{-1} \; ; \quad (16)$$

G_0 is the bare Green's function matrix in orbital space.

Fig. 6 shows the LDOS on a 10×10 square lattice, centered around the cobalt impurity. Note the pronounced peaks at $\vec{r} = (\pm 3a, 0)$, giving rise to the anisotropic dimer structure, observed in[18]. The dimer's size is tied to the magnitude of "reconstructed" nesting vector $\vec{q}_a \approx (0.4\pi, 0)$. Since the cobalt impurity potential is repulsive, LDOS is small at the impurity site and large when $\vec{r} = (\pm a\frac{1}{2}2\pi/0.4\pi, 0) \approx (\pm 3a, 0)$. Therefore, the size of the dimer is $6a$, close to $8a$ of Ref.[18]. In addition, the C_4 symmetry is broken – even if $\Delta_{PoDW} = \Delta_{SDW}$ – due to the different orbital components within each pocket. The charge susceptibility, therefore, peaks along the direction perpendicular to PoDW, and results in the a-axis orientation of the dimer.

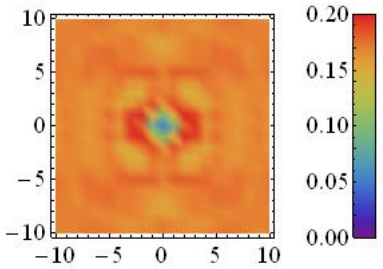

FIG. 6. (Color Online) The LDOS integrated from $E = 0$ to $37meV$[18], with $\Delta_{PoDW} = 20meV$, $\Delta_{SDW} = 15meV$, and the impurity located at $\vec{r} = (0, 0)$. We assume e_y (e_x) couples to h_2 (h_1). LDOS peaks at $\sim \vec{r} = (\pm 3a, 0)$, fixing the dimer size to $6a$. The dimers are aligned with the x axis, reflecting the orientation of the peaks of charge susceptibility (Fig. 5). This anisotropy is due to different magnitudes of DWs order parameters and different orbital content of individual pockets.

In summary, we have shown that the anisotropic electronic dimer structure can be understood based on the "hidden" PoDW order in parent compounds. This order induces a "reconstructed" nesting vector $\vec{q}_a$, at which the charge susceptibility $\chi(\vec{q}_a)$ develops pronounced peaks. Furthermore, the C_4 symmetry is genetically broken due to the orbital components. The dimer, therefore, points along the a axis of AFM order, in accordance with experiments. More generally, our results accentuate the potential of local probes as diagnostic tools in unraveling the patterns of various forms of order in iron pnictides.

We thank Milan Allan and J. C. Seamus Davis and also J. E. Hoffman for discussions and for sharing data with us prior to publication. We thank Pierre Richard and Nachum Plonka for comments. This work was supported in part by the IQM, under Grant No. DE-FG02-08ER46544 by the U.S. DoE, Office of Basic Energy Sciences, Division of Materials Sciences and Engineering.

[1] Y. Kamihara, T. Watanabe, M. Hirano, and H. Hosono, J. Am. Chem. Soc. **130**, 3296 (2008).

[2] M. Rotter, M. Tegel, D. Johrendt, Phys. Rev. Lett. **101**, 107006 (2008).

[3] J. Paglione and R. L. Greene, Nat. Phys. **6**, 645 (2010).

[4] M. A. McGuire, A. D. Christianson, A. S. Sefat, B. C. Sales, M. D. Lumsden, R. Jin, E. A. Payzant, and D. Mandrus, Phys. Rev. B **78**, 094517 (2008).

[5] S. D. Wilson, Z. Yamani, C. R. Rotundu, B. Freelon, E. Bourret-Courchesne, and R. J. Birgeneau, Phys. Rev. B **79**, 184519 (2009).

[6] J. H. Chu, J. G. Analytis, K. De Greve, P. L. McMahon, Z. Islam, Y. Yamamoto, and I. R. Fisher, Science **329**, 824 (2010).

[7] J. J. Ying, X. F. Wang, T. Wu, Z. J. Xiang, R. H. Liu, Y. J. Yan, A. F. Wang, M. Zhang, G. J. Ye, P. Cheng, J. P. Hu, and X. H. Chen, Phys. Rev. Lett. **107**, 067001 (2011).

[8] I. R. Fisher, L.Degiorgi, and Z. X. Shen, Reports on Progress in Physics **74**, 124506 (2011).

[9] T.-M. Chuang, M. P. Allen, J. Lee, Y. Xie, N. Ni, S. L. Bud'ko, G. S. Boebinger, P. C. Canfield, and J. C. Davis, Science **327**, 181 (2010).

[10] M. Yi, D. H. Lu, J.-H. Chu, J. G. Analytis, A. P. Sorini, A. F. Kemper, B. Moritz, S.-K. Mo, R. G. Moore, M. Hashimoto, W. S. Lee, Z. Hussain, T. P. Devereaux, I. R. Fisher, and Z.-X. Shen, PNAS **108**, 6878 (2011).

[11] M. Yi, D. H. Lu, R. G. Moore, K. Kihou, C.-H. Lee, A. Iyo, H. Eisaki, T. Yoshida, A. Fujimori, and Z.-X. Shen, arXiv:1111.6134 (unpublished).

[12] C. de la Cruz, W. Z. Hu, S. Li, Q. Huang, J. W. Lynn, M. A. Green, G. F. Chen, N. L. Wang, H. A. Mook, Q. Si, and P. Dai, Phys. Rev. Lett. **104**, 017204 (2010).

[13] M. G. Kim, R. M. Fernandes, A. Kreyssig, J. W. Kim, A. Thaler, S. L. Bud'ko, P. C. Canfield, R. J. McQueeney, J. Schmalian, and A. I. Goldman, Phys. Rev. B **83**, 134522 (2011).

[14] A. Cano, M. Civelli, I. Eremin, and I. Paul, Phys. Rev. B **82**, 020408 (2010).

[15] R. M. Fernandes, A. V. Chubukov, J. Knolle, I. Eremin, and J. Schmalian, arXiv:1110.1893 (unpublished).

[16] W. Lv, F. Kruger, and P. Phillips, Phys. Rev. B **82**, 045125 (2010); W. Lv, and P. Phillips, Phys. Rev. B **84**, 174512 (2011).

[17] J. Kang and Z. Tešanović, Phys. Rev. B **83**, 020505 (2011).

[18] M. P. Allen, T.-M. Chuang, Y. Xie, J. Lee, N. Ni, S. L. Bud'ko, G. S. Boebinger, Q. Wang, D. Dessau, P. C. Canfield, and J. C. Davis, unpublished.

[19] See also Can-Li Song, Yi-Lin Wang, Ye-Ping Jiang, Lili Wang, Ke He, Xi Chen, Jennifer E Hoffman, Xu-Cun Ma, and Qi-Kun Xue, arXiv:1203.2629 (unpublished).

[20] T. Kondo, R. M. Fernandes, R. Khasanov, C. Liu, A. D. Palczewski, N. Ni, M. Shi, A. Bostwick, E. Rotenberg, J. Schmalian, S. L. Budko, P. C. Canfield, and A. Kaminski, Phys. Rev. B **81**, 060507 (2010).

[21] M. Daghofer, A. Nicholson, A. Moreo, and E. Dagotto, Phys. Rev. B **81**, 014511 (2010).

[22] V. Cvetkovic and Z. Tesanovic, Europhys. Lett. **85**, 37002 (2009).

[23] X.-P. Wang, P. Richard, Y.-B. Huang, H. Miao, L. Cevey, N. Xu, Y.-J. Sun, T. Qian, Y.-M. Xu, M. Shi, J.-P. Hu, X. Dai, and H. Ding, arXiv:1201.3655 and references therein.

[24] A. Nicholson, Q. Luo, W. Ge, J. Riera, M. Daghofer, G. B. Martins, A. Moreo, and E. Dagotto, Phys. Rev. B **84**, 094519 (2011).

[25] The orbital content of h_2 and h_1 being very similar[23], it is the *geometric* nesting that dictates that h_2 – closer in shape to e pockets than h_1 – gets involved in formation of the PoDW. If, however, the roles of h_2 and h_1 were to be reversed, the dimer resonances would align *perpendicular* to AFM, opposite to what is observed. Similar outcome would follow from the reversal of ellipticity of e pockets.

[26] A. F. Kemper, C. Cao, P. J. Hirschfeld, and H.-P. Cheng, Phys. Rev. B **80**, 104511 (2009); T. A. Maier, S. Graser, D. J. Scalapino, and P. J. Hirschfeld, Phys. Rev. B **79**, 224510 (2009).